Research & Reviews: Journal of Material Sciences ISSN: 2321-6212

Influence of (Carboxy Methylcellulose/Poly (Lactic Acid))/Zinc Oxide Nanoparticles Based Composite Coating on *Rhizopus* Rot of Tomatoes during Storage

Salem EA[1], Ahmed Awadallah F[2]*, Maysara E. Aboulfotouh[2], Hussein E Ali[3]

[1]Department of Food Irradiation, National Center for Radiation Research and Technology (NCRRT), Egyptian Atomic Energy Authority (EAEA), Cairo, Egypt
[2]Department of Radiation Research of Polymer, National Center for Radiation Research and Technology (NCRRT), Egyptian Atomic Energy Authority (EAEA), Cairo, Egypt
[3]Department of Radiation Chemistry, National Center for Radiation Research and Technology (NCRRT), Egyptian Atomic Energy Authority (EAEA), Cairo, Egypt

Research Article

Received: 23-Jun-2023, Manuscript No. JOMS-23-103586; **Editor assigned:** 26-Jun-2023, Pre QC No. JOMS-23-103586 (PQ); **Reviewed:** 10-Jul-2023, QC No. JOMS-23-103586; **Revised:** 30-Aug-2023, Manuscript No. JOMS-23-103586 (R); **Published:** 06-Sep-2023, DOI: 10.4172/2321-6212.11.3.009

***For Correspondence:** Ahmed Awadallah F, Department of Radiation Research of Polymer, National Center for Radiation Research and Technology (NCRRT), Cairo, Egypt;

Email: elsheshengy@yahoo.co.uk

Citation: Salem EA, et al. Influence of (Carboxy Methylcellulose/Poly (Lactic Acid))/Zinc Oxide Nanoparticles Based Composite Coating on *Rhizopus* Rot of Tomatoes during Storage. RRJ Mater Sci. 2023;11:003.

ABSTRACT

Nanocomposite films were prepared from graft copolymerization of (carboxymethylcellulose/polylactic acid) using gamma irradiation from ^{60}Co as the main source followed by mixing of Zinc Oxide Nanoparticles (ZnO-NPs) at different concentration. Nanocomposite films of (carboxymethylcellulose/polylactic acid)/(ZnO-NPs) were characterized by different techniques such as FTIR, SEM, XRD, TEM, contact angle, Water Vapor Transmission Rate (WVRT) and mechanical properties. Novelty of present research is using of ZnO-NPs to reduce systematic resistance against tomato fruit rot caused by *Rhizopus stolonifer*. Results showed that the ZnO-NPs at 150 ppm *in vitro* inhibiting the growth of *Rhizopus stolonifer*. In *in-vivo*, equivalent concentration of ZnO-NPs reduces the severity of infection for three weeks under low temperature storage. Through the results displayed that the lowest firmness was for treated with ZnO-NPs, followed by injected samples with *Rhizopus stolonifer*. Further, the similar results were obtained for Total Soluble Solids (TSS) and pH measurements. Therefore, it is deduced that nanocmposite films could be used in coating tomato fruits in a pilot scale.

Keywords: Carboxymethylcellulose; Polylactic acid; Zinc oxide nano-particles; *Rhizopus stolonife*; Tomato fruits

INTRODUCTION

The world population grows yearly, and food demand considered as the biggest challenge nowadays. However, statistics showed that nearly half of the developing nation's population does not have enough and adequate food sources and supplies, partly because of food losses during the post-harvest method. The commodities such as tomatoes can occasionally lose production as high as fifty percent, and such a loss tends to be the highest in countries where the demand for food is much higher [1]. The tomato (*Lycopersicon esculentum*), a world commodity with a high content of vitamins, minerals, and fibers, is potentially consumed. About 162 million tons of tomatoes were produced in the world in 2012. Indonesia ranked 30th with a yearly production of 624,000 tons, Thailand ranked 50th with 270,000 tons yearly, and China was the first producer in rank index with 34 million tons annually [2]. However, around 50% of this production was lost partially due to a lack of proper facilities during storage. Tomato fruits tend to disrupt rapidly and have a very short shelf life, high rate of weight loss, microbial infection, physiological disorders and physical damage [3]. The predominant preservation process in the post-harvest chain uses cold temperatures and high humidity for storage circumstances. Nevertheless, for commodities such as tomato fruits, low temperatures can induce chilling damages [4]. Such a loss can be minimized using an alternative process, which uses Carboxymethyl Cellulose (CMC) as a based coating. Pineapple core which creates waste problems in many countries is a rich source of cellulose and can be a source of CMC. Pineapple can be considered a top commodity production quantity in the world. Thailand and Indonesia can produce 2.7 million tons and 1.8 million tons, respectively, but this potentially creates a waste problem because 55% of the fruit weight is useless, including the core that contains 24.5% cellulose content [5]. CMC has extensively been used in food applications. One of these functions is used as an edible coating for fruits or vegetables to retard water loss (dehydration), providing a permeable barrier to oxygen, moisture and carbon dioxide. The Permeable barrier will also conquer respiration, enhancing the outer textural appearance and quality and helping to keep volatile and flavour compounds [6], therefore it can extend the shelf life of fresh fruits during the transportation process and storage before consumption. There are many applications of CMC as a coating material in food storage. It was found that CMC was able to amend the usual ripening rate of mango up to 32 days at 13ºC [7] and pineapple up to 5 weeks at 10ºC [8], but literature has yet to discuss the effect of CMC based edible coatings for tomato fruits. Many researchers have reported the synthesis of CMC from different agricultural cellulosic waste sources; in contrast, the production of CMC from pineapple core has not previously been reported. However, the adoption rate of Polylactic Acid (PLA) in the food packaging world by manufacturers and brand owners is gradually declining because of its limited applicability and function/performance to cost ratio [9]. PLA has limited applicability to fabricate packaging film for short shelf-life products due to its brittleness and high water vapour permeability. Thus, the blending of low-cost biodegradable polymers or additives to develop functional attributes and performance of PLA while still maintaining its composability at a reasonable cost is demanded to promote bioplastic to replace conventional plastic for food packaging [10,11]. Zhang, et al., studied the blending of Poly (Butylene Adipate-co-Terephthalate) (PBAT) in PLA films to keep the quality of passion fruits during their shelf-life [12]. Their results found that PLA/PBAT film can retard the metabolism of passion fruits and decrease shrinkage index, weight loss, total sugar, firmness, total acid, and ascorbic acid percent. Gamma Irradiation has been used frequently

to create free radical sites on polymer chains. These radicals are active species and can either initiate the polymerization reaction process of a second monomer or recombine again with the growing radical, resulting in the proposed grafts. The irradiation process is sometimes carried out in oxygen isolation media to avoid peroxidation of the trunk polymer chain. One of the advantages is the proxy radical's formation resulted from irradiation of the polymer in the presence of oxygen exposure. Chapiro developed several procedures that are now in public use [13]. Tomato fruit is one of the most potent fruit crops, but the fruit is highly perishable and has a short shelf-life at ambient temperature. Low temperature storage is highly recommended for prolonging shelf-life. However, tomatoes are susceptible to chilling damage. Chilling damage symptoms is a mainly post-harvest problem during the storing process of many horticulture crops. Nanomaterials are defined as material particles with dimensions less than 100 nm. Their functional properties as thermal conductivity, solubility properties, optical properties, and antimicrobial activity have been enhanced. Zinc Oxide Nanoparticles (ZnO-NPs) are one of the most popular nanomaterials nowadays, with remarkable advantages such as abundance, low cost, and high chemical and thermal stability [14]. Furthermore, they have outstanding antifungal and antibacterial activities [15]. According to the FDA regulations regarding zinc oxide safety [16]. ZnO is generally recognized as a safe material, and it can be used as an antimicrobial food additive safely. The application of nanotechnology is a promising technique in the future of crop protection and affords a keener solution for the present problem facing the field of agriculture [17]. Also, recent researches have been focused on producing a safe, edible nano-coating to prolong the shelf life in food preservation of fruits and vegetables. This nano-coating can be applied by several methods as spraying, dipping, brushing or panning technique [18]. Tomato fruits are highly fragile, and large quantities of tomato fruits are wasted due to the unprofessional storage capabilities. It has been calculated that out of 75 lacs tons of the total tomato production in the country, 25 to 30 % will be rotted annually in India due to an excess in the market, inappropriate treatment and improper storage circumstances [19]. The firmness of fruit was found to be 0.62 and 0.67 kg/cm^2 in SEL-7 and ARTH-3, respectively. Gowda, et al. detected that the firmness in eight different diversities of tomato fruits ranged from 4.0 to 8.4 lbs/sq. inch, the lowest fruit firmness was recorded in Pusa Ruby, and the maximum value was in Lerica [20-23].

Therefore, the fundamental aim of this study is to synthesize (carboxymethylcellulose/polylactic acid) and ZnO-NPs nanocomposite films using gamma irradiation and sol-gel approaches, respectively. The nanocomposite films are characterized by different techniques such as FTIR, SEM, XRD, TEM, contact angle, Water Vapour Transmission Rate (WVRT) and mechanical properties. The prepared nanocomposite films are exploited in food packaging as coating films on tomato fruits in order to reduce the systematic resistance against tomato fruit rot caused by *Rhizopus stolonifer*. Furthermore, variable parameters are elaborated in this study and compared to the control on weight loss, texture, redness, Total Soluble Solid (TSS), pH measurements and vitamin C content of cherry tomatoes in ambient storage (25°C and 70% R.H.).

MATERIALS AND METHODS

Materials

Carboxymethyl Cellulose (CMC) (M_w=25,000 g/mol, zinc acetate dihydrate (Zn $(C_2H_3O_2)_2.2H_2O$) and polylactic acid M_w=60,000 (g/mol) were supplied from Sigma-Aldrich (USA) and Sigma-Aldrich (Germany). The tomato's fruits (*Solanum Lycopersicon* L) were supplied from the local market during the harvest season in 2019/2020. Lab experiments were carried out at the lab of the food Irradiation department in the Egyptian atomic energy authority.

Sol-gel synthesis of ZnO-NPs

The ZnO-NPs were prepared by sol-gel technique. 5 g of zinc acetate dihydrate (Zn $(C_2H_3O_2)_2.2H_2O$) is transferred to 150 ml

beaker then 100 ml of deionized water was added into a 250 cm^3 beaker. The mixture solution was stirred gently *via* a magnetic stirrer at 150 rpm for 30 min. 0.5 M Sodium Hydroxide (NaOH) was added drop wise to the mixture solution to attain the desired pH of 8 level [24]. The mixture was stirred magnetically for 5 min, and the precipitate was clarified with Whatman No. 1 filter paper. The residue was washed by deionized water and then ethanol to exclude the fine traces of the unreacted materials. The final product was placed into an oven to be dried at 105°C for 24 h, and finally, the gel was formed. Calcination was completed for 12 h at 130°C. The ZnO-NPs (wurtzite structure) were formed. Moreover, a proposed reaction mechanism of ZnO-NPs formation is shown in Figure 1. Comprehensive studies evaluation settles that sol-gel is the usually nominated process for producing ZnO-NPs. This is because this method yields outstanding tight particle size distribution and well-defined crystalline structure. This technique needs low-temperature, simple composition control with considering cost effectiveness (Figure 1).

Figure 1. A proposed reaction mechanism of ZnO-NPs formation.

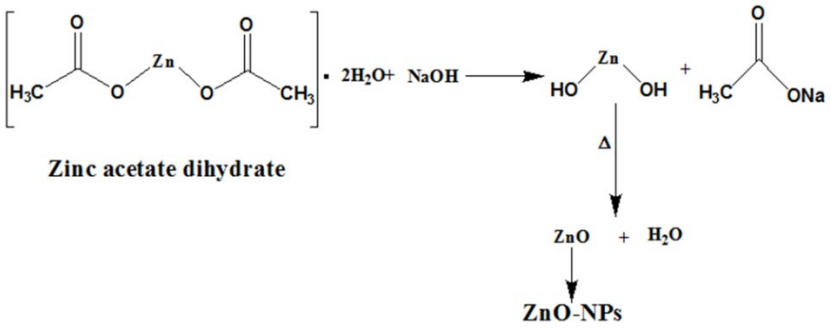

Synthesis of CMC-graft-PLA copolymer

The CMC graft poly (lactic acid) (CMC-g-PLAc) copolymer was obtained via gamma irradiation technique. In addition, the sample of CMC-g-PLAc will be called after later as CMC-g-PLAc. In this process, PLA was mixed with CMC with a specific equal molar ratio of (*i.e.,* 6 g of PLA to 2.5 g CMC). 6 g of PLA was added to chloroform (100 ml) and complete dissolution was achieved by reflux during stirring at 60°C for 24 h. Next, 2.5 g of CMC was added to the dissolved PLA and continued refluxing with stirring for 24 h at 60°C. After that, the mixture of CMC/PLA was sonicated at 50°C for 45 min in purpose of enhancing the dispersion of CMC into PLA solution [25]. After this, the dissolved mixture was exposed to gamma irradiation at 10 kGy of radiation dose rate ~0.9 kGy/h (Indian gamma cell). This value of radiation dose was chosen according to the study of Fekete et al., that tackled the effect of radiation dose on the structure of CMC and starch [26]. Moreover, the suggested reaction mechanism of graft copolymerization of PLA and CMC is depicted in Figure 2. This is a proposed reaction mechanism is agreement with a reported in literature studies elsewhere [27,28].

Figure 2. A proposed reaction mechanism of CMC-g-PLAc graft copolymer formation.

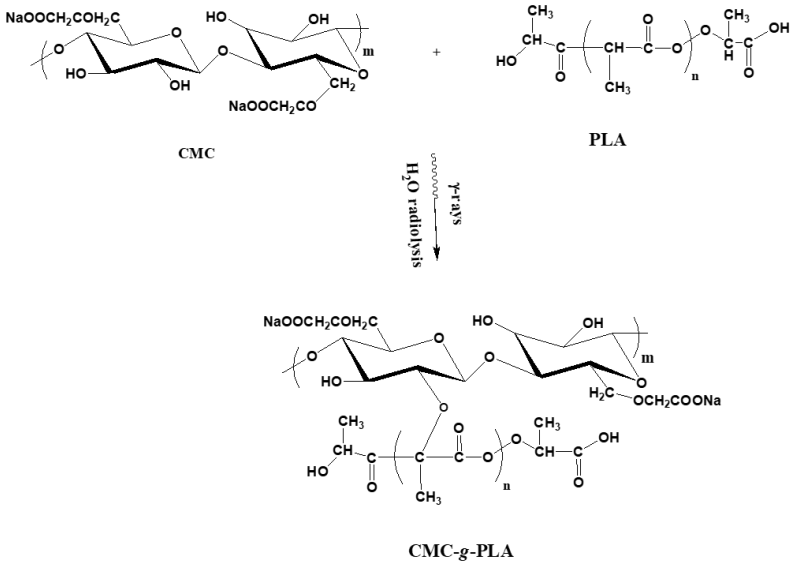

Synthesis of CMC-g-PLAc/ZnO-NPs nanocomposite and coating process

Series of ZnO-NPs concentrations as solutions were prepared from 0, 50, 100 and 150 ppm (with adjusted pH level to 4), then were added to the irradiated solution of CMC-g-PLA, respectively and stirred magnetically for 24 h at 40°C using magnetic stirrer to guarantee the good distribution of ZnO-NPs into the matrix of CMC-g-PLAc. The solution of CMC-g-PLAc/ZnO-NPs nanocomposite is ready to be utilized for coating process the tomato fruits. In addition, Figure 3 illustrate the schematic diagram for the coating process of CMC-g-PLA0ZnO-NPs composite solution onto surface of tomato fruits, as shown below. The assigned samples are coded as CMC-g-PLAc-ZnO-NPs-0, CMC-g-PLAc-ZnO-NPs-50, CMC-g-PLAc-ZnO-NPs-100 and CMC-g-PLAc-ZnO-NPs-150 nanocomposites (Figure 3).

Figure 3. A proposed schematic diagram for the coating process of CMC-g-PLAc/ZnO-NPs nanocomposite onto surface tomato fruit.

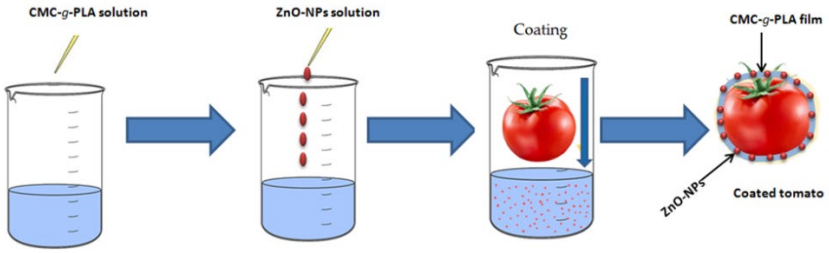

Water vapour transmission rate

The Water Vapour Transmission Rate (WVTR) of CMC-g-PLAc-ZnO-NPs-0, CMC-g-PLAc-ZnO-NPs-50, CMC-g-PLAc-ZnO-NPs-100 and CMC-g-PLAc-ZnO-NPs-150 nanocomposite films was estimated via the approach reported elsewhere [29]. The nanocomposite films were put at the mouth of bottle with a diameter equal to 15 mm that involving 10 ml of distilled water. The bottles were initially weighed as W_o and followed by transferring the nanocomposite films into an incubator at 37°C for 24 h. The weight of the container was determined as W_1 and the value of WVTR was calculated based on the below formula of Equation 1. The symbol of "A" denotes to the mouth area of bottle by m^2. All calculated values are conducted by

considering as the mean ± standard deviation (n=3).

$$\text{WVTR} = \left(\frac{W_o - W_1}{A \times 24}\right)\frac{g}{m^2\text{h}} \qquad (1)$$

Fungal species, culture media and pathogenicity test

Rhizopus stolonifer was prepared by the fungal disease research division, the plant pathology research institute, agricultural research centre, Giza, Egypt. The fungus were isolated and sustained on (PDA) Potato Dextrose Agar medium and recognized on Czapek's medium. Growth inhibition, other physiological research and samples for microscopical studies were carried out on Czapek's broth medium. The preparation of details media were found elsewhere [30]. Healthy Tomato fruits were wisely rinsed well with disinfected water, then kept to dry at ambient temperature, surface sterilized by 70% ethyl alcohol for a short time, almost one minute. Minor wounds were formed on each Tomato's surface and injected by fungus using equal parts of mycelial disks (3 mm in diameter each) obtained from 7 days old PDA cultures, and then one disk sample of 3 mm was placed in each scratch. Check handlings were likewise carried out through the fungal free medium. Three replicates samples were carried out for each treatment, and each containing ten fruits was used to be confident with the results. For each handling, the injected tomato fruits were put in a disinfected carton box with a 5 kg capacity and retained at room temperature for 7 days. The decay index and severity of infection percent were used to calculate the resulting rot, according to Chastanger and Ogawa [31]. Using the visual inspection of the naked eye of each fruit infection. Infected fruits were categorized into five categories: 0=Superficial flack (no rot), 1=1-24% of the surface decayed, 3=50-74% of the surface decayed, 2=25-49% of the surface decayed 4=75% or more of the surface decay. The Decay Index (DI) for each treatment was calculated according to equation 2 and the severity of in infection was determined according to equation 3.

$$\text{DI} = \frac{sum(nunmber\ of\ fruits\ per\ category\ \times category\ number)}{Total\ number\ of\ fruits\ infected} \quad g/m^2h \qquad (2)$$

$$\%(\text{severity of infection}) = \left(\frac{DI}{4}\right) \times 100 \qquad (3)$$

Firmness measurement

Tomato fruit firmness assessment was accomplished using a T.A. XTPlus texture analyzer (Stable Micro Systems Ltd., Godalming, U.K.). The maximum penetration force for a probe with a 4 mm diameter to penetrate a tomato's fruit to a depth of 5 mm at a rate of 5 mm/s was measured. Tomato fruit was placed perpendicular to the probe to permit penetration in their center, and the units were expressed in Newton (N). Ten fruits from each treatment procedure were measured.

Total soluble solids measurement

The Total Soluble Solids (TSS) measurement content of the fruit was detected using a refractometer (Atago Co., Tokyo, Japan). A sample was prepared by mixing the tomato fresh in a blender. The sample was homogenously mixed, a few drops were taken on a prism of the refractometer, and results were determined by reading the scale in the meter as defined elsewhere [32].

pH measurement

The pH of the tomato fruits samples was detected by the direct method described elsewhere [33]. The pH was attained in 10

mL of standardized pulp and added to 100 ml of distilled water. The solution was engaged to a digital potentiometer, adjusted with pH 4.0 and 7.0 buffer solutions.

Characterization

The infrared spectra were investigated by Fourier Transform Infrared (FTIR) spectrophotometer, Perkin Elmer, USA, with a range of 4000–400 cm^{-1}. EDX analysis is conducted using energy dispersive X-ray unit microprobe EDX (Zeiss Smart EDX) coupled with Scanning Electron Microscope (SEM) that used to investigate the changes in the morphology of samples. A JEOL JSM- 7100F (JEOL, Tokyo, Japan) field-emission scanning electron microscope is utilized for this investigation. X-Ray Diffraction (XRD) patterns of the selected samples were detected by an X-ray diffractometer (a Shimadzu XRD 600). XRD patterns were acquired at a scan rate of 5° min^{-1} on the diffractometer with CuKα radiation source, a generator voltage of 40 kV, a generator current of 40 mA and a wavelength of 0.1546 nm at ambient temperature. All the diffraction patterns were examined at ambient temperature and under certain operating circumstances. The shape and particle size were detected using Transmission Electron Microscopy (TEM) (JEOL JSM- 100 CX, Shimadzu Co., Japan) with an acceleration voltage of 80 kV. Mycelia of *Rhizopus stolonifer* grown in P.D. broth medium treated with Zn-NPs and that from non-treated (control) were immersed in 2.5% glutaraldehyde at 4°C for 24 hours and post fixed in 1.0% osmium tetra oxide for one hour at ambient temperature. The specimens were then dehydrated with ascending acetone concentrations, critical point dried, and finally sputter coated with gold. The investigation and Imaging were done through Joel Scanning Electron Microscope (JSM–1200 EX). A Phoenix 300 contact angle goniometer (SEO Co. Ltd., Suwon, South Korea) is utilized to determination the contact angles of CMC-g-PLAc-ZnO-NPs-0, CMC-g-PLAc-ZnO-NPs-50, CMC-g-PLAc-ZnO-NPs-100 and CMC-g-PLAc-ZnO-NPs-150 nanocomposite films. The measurements of mechanical properties of CMC-g-PLAc-ZnO-NPs-0, CMC-g-PLAc-ZnO-NPs-50, CMC-g-PLAc-ZnO-NPs-100 and CMC-g-PLAc-ZnO-NPs-150 evaluated by a microprocessor controlled tensile testing apparatus (Hung-Ta Model HT-9112, Taiwan).

In vitro effect of CMC-g-PLAc- ZnO-NPs on *Rhizopus stolonifer*

The antifungal activity of ZnO-NPs against *Rhizopus stolonifer* was identified by the process of Singh, et al [34]. Autoclaved PDA media were transferred into 90 mm petri dish plates. A mycelium disk cut (5 mm diameter) from 10 days old culture of *Rhizopus stolonifer* grown on PDA was placed on the center of the Petri plate. PDA was cured with a solution of CMC-g-PLAc-ZnO-NPs containing 50, 100 and 150 ppm of ZnO-NPs in addition to the control treatment. The selected treatment doses were poured into the media.

In vivo effect of CMC-g-PLAc- Zn-NPs on *Rhizopus stolonifer*

In vivo effect of ZnO-NPs behaviour in adjusting the post-harvest spoilage of tomato fruits induced by *Rhizopus stolonifer* as disease severity percentages. Tomato fruits were immersed in CMC-g-PLAc-ZnO-NPs-0, CMC-g-PLAc-ZnO-NPs-50, CMC-g-PLAc-ZnO-NPs-100 and CMC-g-PLAc-ZnO-NPs-150 solutions for 3 min for coating the surface of tomato fruits and air dried for two hours in a laminar flow hood. Tomato fruits were packed in plastic bags, placed in a sanitized carton box and reserved for 1-3 weeks in cold conditions at 13°C and 90-95 humidity %. Moreover, for each handling, three repeated replicates, including 10 tomato fruits, were conducted; the results were registered as an infection severity.

RESULTS AND DISCUSSION

Figure 4 (a) shows the FTIR of the prepared ZnO-NPs by the sol-gel process in the range of 4000–400 cm^{-1}. FTIR spectrum

represents the wavenumbers range from 400 cm^{-1} to 4000 cm^{-1}, which confirms the essential stretching modes of metal oxides between 400 cm^{-1} and 800 cm^{-1} [35]. The peaks at 3413 and 1645 cm^{-1} are referred to as O–H stretching vibration and H–O–H bending vibration, respectively, which are attributed to the small amount of H_2O molecules found in pure ZnO-NPs, which may be due to the existence of moisture [36]. The peak at 2341 cm^{-1} has been attributed to CO_2 molecules in the instrument's atmosphere and/or media [37]. Therefore, FTIR results displayed the high purity of the prepared ZnO-NPs [38]. Figure 4 (b) displays the SEM photomicrograph of pure ZnO-NPs. It can observe that the formation of nanoparticles of Zn with spherical shape. Moreover, the outcome results determined that the average particle size of Zn-NPs is 22.8 ± 4.9 nm. Additionally, the EDX analysis in Table 1 shows the elements percentages found in pure ZnO-NPs-0. As noted in the outcome results, the only elements found in nancomposite were O and Zn, which refers to elements, existed in the prepared inorganic nanomaterials.

Figure 4. (a) FTIR spectrum; and (b) SEM photomicrograph of the prepared ZnO-NPs *via* the sol-gel method.

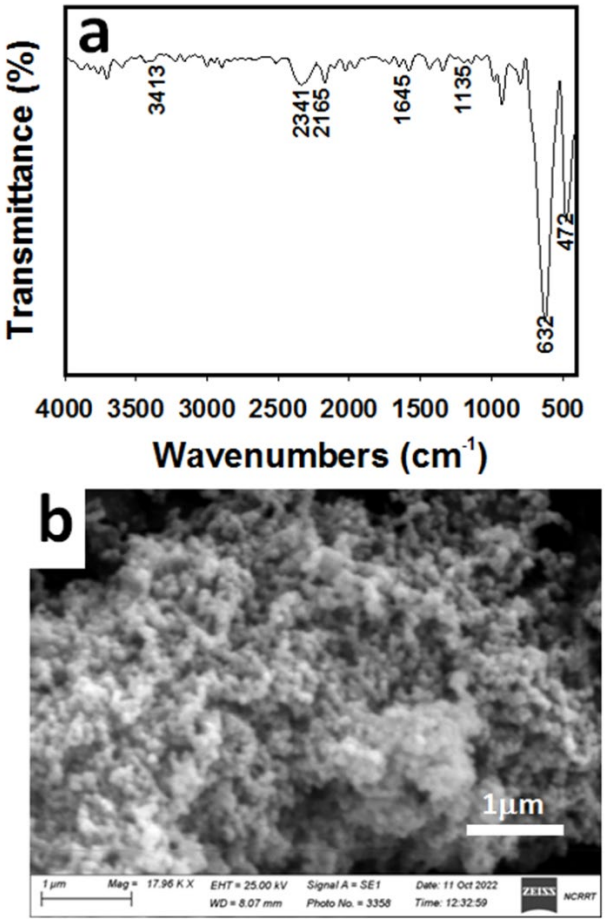

Figure 5(a) represents the FTIR of the CMC-g-PLAc film. It was observed that the dominant peaks of CMC at 3461 cm^{-1} (O–H stretching overlapping N–H stretching of primary amine), 2938 cm^{-1} (C–H stretching vibration of CH_2 symmetry), 1640 cm^{-1} (C=O stretching of amide bonds), 1376 cm^{-1} (asymmetrical C–H bending of CH_2 group), 1039 cm^{-1} (C–O–C bridge stretching), and 1120 cm^{-1} (C_3–O stretching) [39,40]. The existence of PLA displays the dominant peak at 1725 cm^{-1} (stretching vibration of the carbonyl group (–C=O) from the repeated ester group), 2938 cm^{-1} and 2884 cm^{-1} (asymmetric and symmetric vibration of –C.H– from $–CH_3$ groups in the side chains) [41,42]. Therefore, both CMC and PLA were found in

the prepared film. Figure 5 (b) exposes the SEM photomicrographs of CMC-g-PLAc film. It was observed that the image of CMC-g-PLAc film is empty of ZnO-NPs, as depicted in Figure 5b. Additionally, the EDX analysis in Table 1 shows the elements percentages found in CMC-g-PLAc-ZnO-NPs-0, CMC-g-PLAc-ZnO-NPs-50, CMC-g-PLAc-ZnO-NPs-100 and CMC-g-PLAc-ZnO-NPs-150 nancomposite films. As seen in the outcome results, the only elements found in nancomposite films were C, O, and Zn, which refers to elements existed in nancomposite films.

Figure 5. (a) FTIR spectrum; and (b) SEM photomicrograph of the CMC-g-PLAc film at radiation dose 10 kGy of radiation dose rate ~0.9 kGylh.

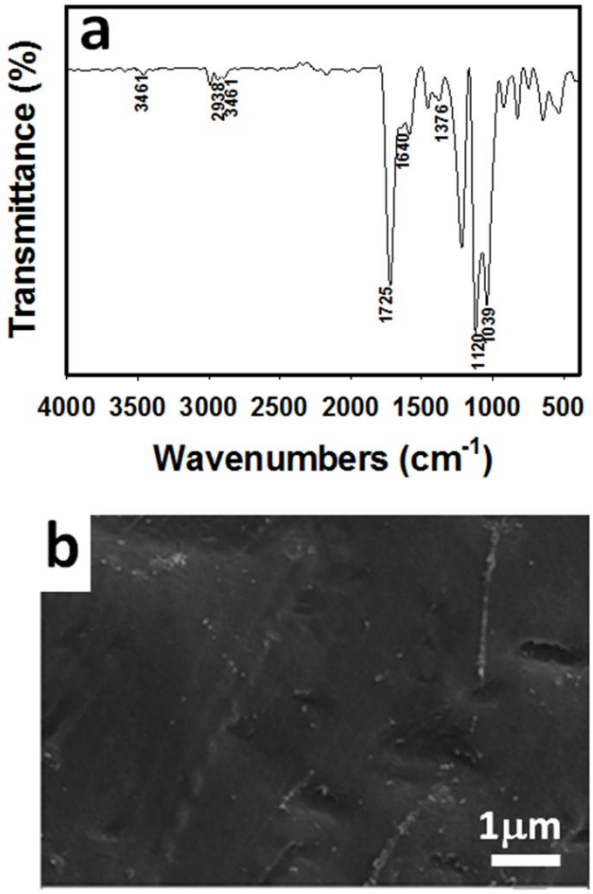

Table 1. EDX analysis of pure ZnO-NPs and CMC-g-PLAc-ZnO-NPs-0, CMC-g-PLAc-ZnO-NPs-50, CMC-g-PLAc-ZnO-NPs-100, and CMC-g-PLAc-ZnO-NPs-150 nancomposite films.

Sample	Weight (%)		
	Zn	O	C
ZnO-NPs	55.32	44.68	0
CMC-g-PLAc-ZnO-NPs-0	0	42.67	57.33
CMC-g-PLAc-ZnO-NPs-50	1.53	43.13	55.34
CMC-g-PLAc-ZnO-NPs-100	2.41	46.13	51.46
CMC-g-PLAc-ZnO-NPs-150	3.81	48.13	48.06

Figure 6 shows the X-ray diffraction pattern of CMC-g-PLAc-ZnO-NPs-50 and CMC-g-PLAc-ZnO-NPs-150 nanocomposites. The broadening line of the XRD peaks explains that the synthesized material contains particles in the nanoscale. We identified

peak intensity, location and width, and Full Width at Half Maximum (FWHM) data from this XRD patterns analysis. The diffraction peaks at 31.84°, 34.52°, 36.33°, 47.63°, 56.71°, 62.96°, 68.13°, and 69.18° have been interpreted the nanomaterials fingerprint as hexagonal wurtzite phase of ZnO [43,44], with lattice constants a=b=0.324 nm and c=0.521 nm (JPCDS card number: 36-1451) [45], and further, it approves that the synthesized ZnO nanopowder was free of impurities and pure. XRD peaks do not contain any other characteristic peaks than ZnO peaks. The synthesized Zn-NPs diameter was determined by the Debye-Scherrer formula [46],

$$d = \frac{0.89\lambda}{\beta \cos\theta},$$

Where 0.89 is Scherrer's constant, θ is the Bragg diffraction angle, λ is the wavelength of X-rays and β is the (FWHM) full width at half-maximum of the diffraction peak equivalent to the plane (101). (FWHM) is used to measure the sample's average particle size, which was 16.21 nm. The FWHM considered the more intense peaks assigned to (101) plane located at 36.33° using Scherrer's formula.

Figure 6. XRD patterns of CMC-g-PLAc-ZnO-NPs-50 (black line) and CMC-g-PLAc-ZnO-NPs-150 (red line) nanocomposite films. Radiation dose 10 kGy of radiation dose rate ~0.9 kGy/h.

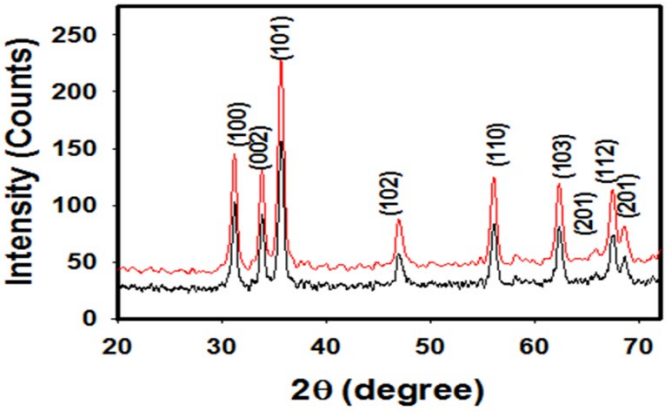

Figure 7 (a-d) represents the TEM photomicrographs of (a) CMC-g-PLAc-ZnO-NPs-50, (b) CMC-g-PLAc-ZnO-NPs-100, (c) CMC-g-PLAc-ZnO-NPs-150 nanocomposites and (d) pure ZnO-NPs, respectively. Overall, it can be observed that the distributions of ZnO-NPs into the nanocomposite films are in a proper manner (Figure 7 (a-c)). In contrast, the distribution of ZnO-NPs in pure Zn-NPs between good distribution in some regions in film and other regions featured with aggregated nanoparticles (Figure 7d). In addition, it was observed from Figure 8 that the average particle size of nanoparticles increases with increasing the Zn molecules in in-situ media of reaction. Further, the average particle size of nanoparticles of ZnO-NPs, CMC-g-PLAc-ZnO-NPs-50, CMC-g-PLAc-ZnO-NPs-100 and CMC-g-PLAc-ZnO-NPs-150 are 22.8 ± 4.9, 41.9 ± 5.4, 44.8 ± 4.5 and 51.8 ± 6.3 nm, respectively.

Figure 7. TEM photomicrographs of (a) CMC-g-PLAc-ZnO-NPs-50; (b) CMC-g-PLAc-ZnO-NPs-100; (c) CMC-g-PLAc-ZnO-NPs-150 nanocomposite films; and (d) Pure ZnO-NPs. Radiation dose 10 kGy of radiation dose rate ~0.9 kGy/h.

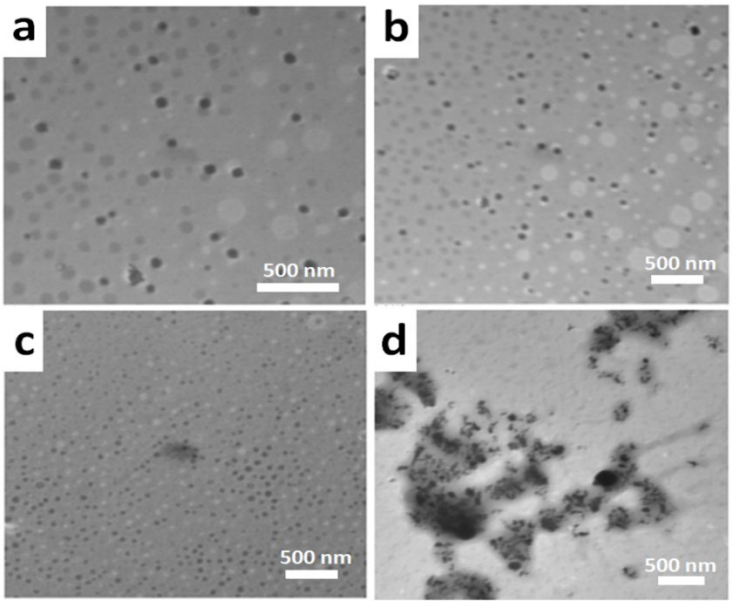

Figure 8. Relationship between particle size and nanocomposite type of CMC-g-PLAc-ZnO-NPs-50, CMC-g-PLAc-ZnO-NPs-100, CMC-g-PLAc-ZnO-NPs-150 and pure ZnO-NPs. Radiation dose 10 kGy of radiation dose rate ~0.9 kGy/h.

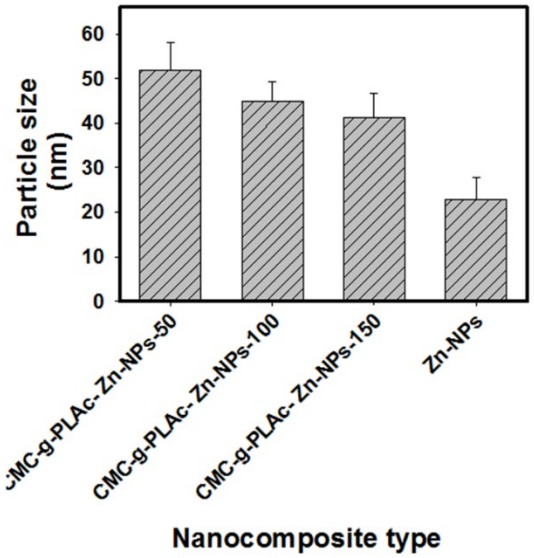

Contact angle is one of the common approaches to conduct the wettability of a surface film. Wetting indicates to the investigation of how a liquid adhered on a solid or liquid spreads out or the capability of liquids to generate the surfaces of boundarys with solid surface. The value of wetting is estimated by determining the contact angle that the liquid forms in contact with the solids or liquids. The wetting value depends on surface tension that leads to augment the contact angle value. A wetting liquid is a liquid that forms a contact angle with the solid surface that is smaller than 90°, where, a nonwetting liquid creates a contact angle between 90 and 180° with the solid [47]. The conventional definition of a contact angle is the angle a liquid creates with the solid or liquid when it is deposited on it. In addition, the contact angle of the

membrane surface shows the hydrophilic (*i.e.,* contact angle <90°) or hydrophobic (*i.e.,* contact angle >90°) features [48]. Figure 9 shows the contact of CMC-g-PLAc-ZnO-NPs-0, CMC-g-PLAc-ZnO-NPs-50, CMC-g-PLAc-ZnO-NPs-100 and CMC-g-PLAc-ZnO-NPs-150 nanocomposite films using deionized water. The CMC-g-PLAc-ZnO-NPs-0 nanocmposite films exposed a water contact angle of 40 ± 3.1°. With augmenting ZnO quantity [49], the water contact angle increased from 65 ± 2.5° to 79 ± 2.7°, referring to augmentation in the hydrophobicity of the CMC-g-PLAc-ZnO-NPs-0 nanocomposite film. This is due to generate stronger bonds between polymeric composite film and ZnO-NPs. This decreases the voids available onto the surface of composite film that leads to restrict the capability of surface of composite film to absorb water molecules. Consequently, the surface of composite film is less able to conserve its hydrophilicity [50].

Figure 9. Water contact angle measurements of CMC-g-PLAc-Zn-NPs-0, CMC-g-PLAc-ZnO-NPs-50, CMC-g-PLAc-ZnO-NPs-100, CMC-g-PLAc-ZnO-NPs-150 nanocomposite films. Radiation dose 10 kGy of radiation dose rate ~0.9 kGy/h.

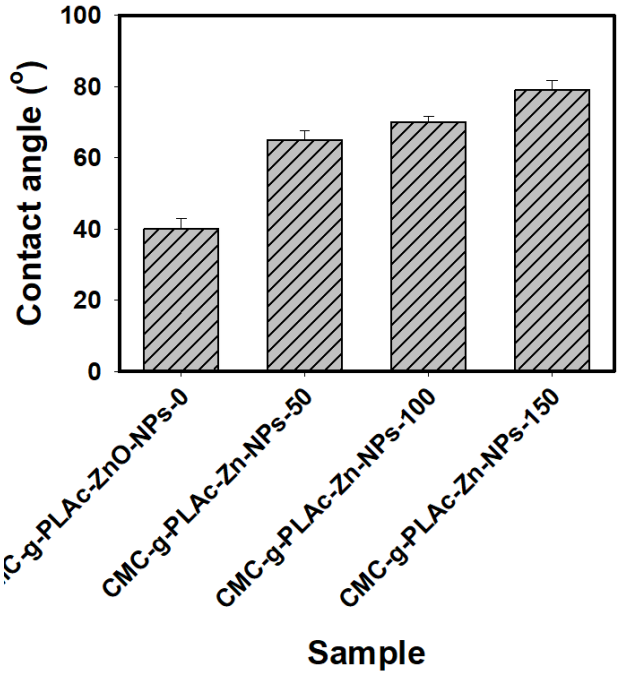

A low value of WVTR for packaging films refers to that the films are good convenience for conserving the quality of food [51]. Figure 10 shows the WVTR values for CMC-g-PLAc-ZnO-NPs-0, CMC-g-PLAc-ZnO-NPs-50, CMC-g-PLAc-ZnO-NPs-100, CMC-g-PLAc-ZnO-NPs-150 nanocomposite films. The addition of ZnO-NPs significantly reduced the values of WVTR. Therefore, the presence of ZnO-NPs can enhance the film's barrier ability against water vapor transmission process. This is attributed to the strong wetting of CMC-g-PLAc films with ZnO-NPs generated more tortuous tracks for transmission of water vapor to pass through the films. Therefore, it can be deduced that the higher ZnO-NPs content either decreases or maintains the same free volume and does not create additional pore size. This leads to reduction of permeability process for moisture. This outcome result is agreement with the result obtained and discussed earlier in experiment of water contact angle. Moreover, the addition of ZnO-NPs makes CMC-g-PLAc more hydrophobic, and as a result, the process of whole moisture permeability reduces [52].

Figure 10. Water Vapor Transmission Rates (WVTR) of CMC-g-PLAc-ZnO-NPs-0, CMC-g-PLAc-ZnO-NPs-50, CMC-g-PLAc-ZnO-NPs-100, CMC-g-PLAc-ZnO-NPs-150 nanocomposite films. Radiation dose 10 kGy of radiation dose rate ~0.9 kGy/h.

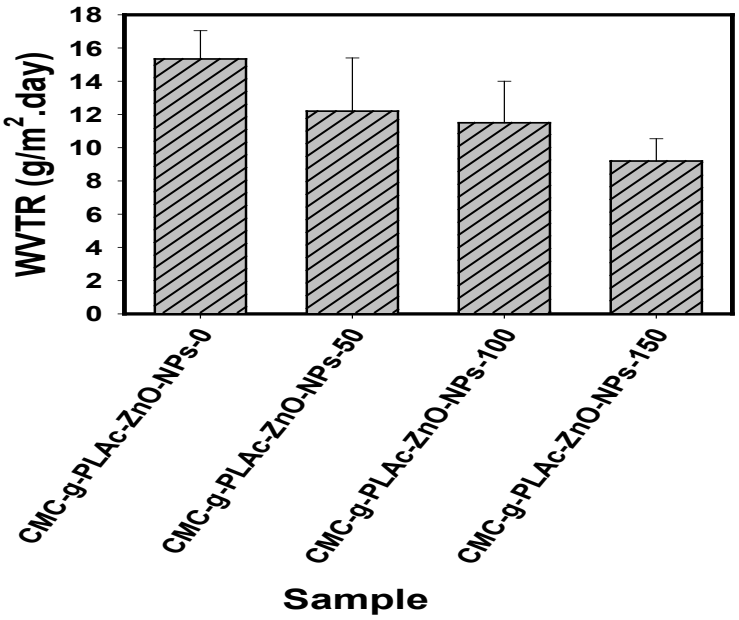

Figure 11 (a, b) shows the tensile strength (MPa) and elongation at break (%), respectively values of CMC-g-PLAc-ZnO-NPs-0, CMC-g-PLAc-ZnO-NPs-50, CMC-g-PLAc-ZnO-NPs-100, CMC-g-PLAc-ZnO-NPs-150 nanocomposite films. Overall, it can be observed from Figure 10a that tensile strength of CMC-g-PLAc-ZnO-NPs-0, CMC-g-PLAc-ZnO-NPs-50, CMC-g-PLAc-ZnO-NPs-100, CMC-g-PLAc-ZnO-NPs-150 nanocomposite films increases by increasing the content of ZnO-NPs. In addition, the lowest and the highest values of tensile strength are 26.32 ± 3.46 and 34.6000 ± 2.71 (MPa) for the corresponding nanocomposite films of CMC-g-PLAc-ZnO-NPs-0 and CMC-g-PLAc-ZnO-NPs-150, respectively. This is assigned to the reinforcement of ZnO-NPs into the composite films that support the formation of stronger intermolecular forces between the CMC-g-PLAc film chains [53]. The molecular force increases when ZnO-NPs react with the hydroxyl group of CMC and PLAc to generate physical bonds such hydrogen bonds [54]. Generally, the nano-filler with greater surface area improve the interaction between NPs and chains of CMC-g-PLAc, therefore improving the formation of crosslinking between CMC-g-PLAc chains [55]. Further, the nanocomposite films are with high concentration of ZnO-NPs exposed a more compact structure that employs to the formation of stronger nanocomposite films. Figure 10b shows elongation at break (%) of CMC-g-PLAc-ZnO-NPs-0, CMC-g-PLAc-ZnO-NPs-50, CMC-g-PLAc-ZnO-NPs-100, CMC-g-PLAc-ZnO-NPs-150 nanocomposite films. Overall, it was seen that the elongation at break decreases by increasing the content of ZnO-NPs into the matrix of CMC-g-PLAc film. This reduction was conducted by incorporating the ZnO-NPs into the film matrices that limit the movement of macromolecules and reduces the elongation capability of films chains [56]. In addition, the incorporation of NPs in film improves the formation of hydrogen bonds between the NPs and functional constituents into film materix, resulting in the formation of compact structure [57].

Figure 11. (a) Tensile strength; and (b) Elongation at break of CMC-g-PLAc-ZnO-NPs-0, CMC-g-PLAc-ZnO-NPs-50, CMC-g-PLAc-ZnO-NPs-100, CMC-g-PLAc-ZnO-NPs-150 nanocomposite films. Radiation dose 10 kGy of radiation dose rate ~0.9 kGy/h.

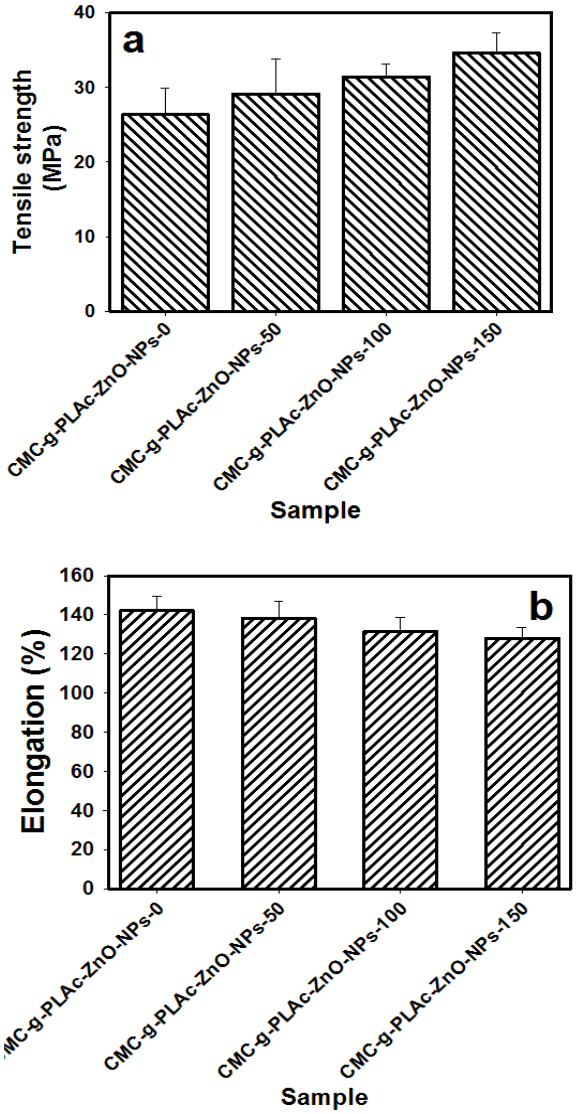

Results obtained in Table 2 showed that as the concentration of Zn-NPs increase, the linear growth of *Rhizopus stolonifer* decrease, and at 150 ppm concentration of ZnO-NPs inhabit the linear growth of *Rhizopus stolonifer*. Further, results obtained in Table 2 showed that the *in-vivo* contact effect of ZnO-NPs on post-harvest tomato rots caused by *Rhizopus stolonifer* as the concentration of ZnO-NPs increases, the severity of infection decreases in different storage periods weeks. ZnO-NPs at 150 ppm concentration prevent the severity of infection till 4 weeks of storage. Moreover, Table 2 exposes the effect of Zinc Nanoparticles on the severity of infection percentages of *Rhizopus* rot of Tomato fruits initiated by *Rhizopus stolonifer* during cold storage. It noted there are no disease severity percentages of *Rhizopus* rot in Tomato fruit preserved by ZnO-NPs during cold storage. For tomato fruits treated by ZnO-NPs+ injected, there was no severity of infection until the 4 weeks under cold storage. For the tomato fruits un-treated (control), it was found that the severity percentages increased from (18 to 75%) during cold storage. Previous results showed that the severity of infection was 18, 40, 55.5 and 75% after 1, 2, 3 and 4 weeks of cold storage of tomato fruits (control). In contrast, the disease severity was 7.5, 12.5, 16.0 and 30%

after 1, 2, 3 and 4 weeks of cold storage of tomato fruits which were inoculated and treated with 50 ppm ZnO-NPs. Also, the disease severity was 3.0, 5.3, 9.0 and 14.5% after 1, 2, 3 and 4 weeks of cold storage of tomato fruits which were injected and treated with 100 ppm ZnO-NPs. However, at 150 ppm of ZnO-NPs, there is no severity of infection till the fourth week of cold storage.

Table 2. *In vitro* contact, the effect of CMC-g-PLAc-ZnO-NPs nanocomposite films on linear growth of *Rhizopus stolonifer* and on post-harvest tomato rots caused by *Rhizopus stolonifer*.

Sample	ZnO-NPs (ppm)		Linear growth (cm)	
CMC-g-PLAc-ZnO-NPs-0	0		9	
CMC-g-PLAc-ZnO-NPs-50	50		5	
CMC-g-PLAc-ZnO-NPs-100	100		2	
CMC-g-PLAc-ZnO-NPs-150	150		0	
Sample	The severity of infection during the different storage periods (%) (weeks)			
	1	2	3	4
CMC-g-PLAc-ZnO-NPs-0	18	40	55.5	75
CMC-g-PLAc-ZnO-NPs-50	7.5	12.5	16	30.5
CMC-g-PLAc-ZnO-NPs-100	3	5.3	9	14
CMC-g-PLAc-ZnO-NPs-150	0	0	0	0

Table 3 shows the superiority of tomato fruits treated by CMC-g-PLAc-ZnO-NPs-150 and injected by *Rhizopus stolonifer* comparison with an untreated sample (control) during cold storage. It was noticed that the firmness values decreased of (520, 500, 440, and 415 N), (450, 420, 380, and 306 N), (530, 512, 450, and 424 N), and (480, 440, 390, and 379 N) by increasing cold storage period of (1, 2, 3 and 4 weeks) for (untreated) control, inoculated, CMC-g-PLAc-ZnO-NPs-150 CMC-g-PLAc-Zn-NPs-150+ inoculated by *Rhizopus stolonifer* of tomato treatments, respectively. Further, Table 3 represents the Total Soluble Solids (TSS) of the tomato fruits ranged from 4.5 in control fruits after one week of cold storage to 2.7 after 4 weeks. The maximum TSS value among the treated fruits was detected in CMC-g-PLAc-ZnO-NPs-150 (4.4), followed by inoculated + Injected by fungi (4.2). Also, it was observed that by increasing the cold storage time (from 1 to 4 weeks), there was a decrease in TSS (from 4.5 to 2.7 %), (from 4.0 to 2.1 %), (from 4.4 to 2.5 %) and (from 4.2 to 2.3 %) for (untreated) control, CMC-g-PLAc-ZnO-NPs-150 and CMC-g-PLAc-ZnO-NPs-150+ inoculated then injected by *Rhizopus stolonifer* of tomato treatments, respectively after 4 weeks of cold storage.

Table 3. Effect of different samples on the firmness and Total Soluble Solids (TSS) of tomato's fruits with *Rhizopus stolonifer* and under cold storage.

	Firmness (week)			
Sample	1	2	3	4
(Control)	520	500	440	415
Inoculated	450	420	380	306
CMC-g-PLAc-ZnO-NPs-150	530	512	450	424
CMC-g-PLAc-ZnO-NPs-150+inoculated	480	440	390	379
	TSS (week)			
Sample	1	2	3	4
(Control)	4.5	4.1	3.1	2.7
Inoculated	4	3.6	2.2	2.1

CMC-g-PLAc-ZnO-NPs-150	4.4	4	3	2.5
CMC-g-PLAc-ZnO-NPs-150+inoculated	4.2	3.8	2.4	2.3

Table 4 exposed that the pH of the control (untreated) fruits decreased from 3.5, 2.6, 1.8, and 1.4 in various storage times (1, 2, 3 and 4 weeks), respectively. The maximum pH value among the treated tomato fruits was detected in CMC-g-PLAc-ZnO-NPs-150 (3.4), followed by treatment of CMC-g-PLAc-ZnO-NPs-150 + Injected by *Rhizopus stolonifer* (2.8). Also, it was observed that by increasing the cold storage period from 1 to 4 weeks, there was a decrease in pH (from 2.5 to 1.1 value), (from 3.4 to 1.3 value) and (from 2.8 to 1.2 value) for injected by *Rhizopus stolonifer*, CMC-g-PLAc-ZnO-NPs-150 + Injected by *Rhizopus stolonifer*, respectively, compared to untreated sample (control), which declined (from 3.5 to 1.4 value). Further, for the pH value of tomato fruits, it was represented that the pH values were decreased (3.5, 2.6, 1.8, and 1.4 values), (2.5,1.8,1.1 and 1.1 values), (3.4, 2.4, 1.6 and 1.3 value) and (2.8, 1.9, 1.4, and 1.2 value) by increasing cold storage period for (1, 2, 3 and 4 days) for un-treated sample (control), inoculated, CMC-g-PLAc-ZnO-NPs-150 and CMC-g-PLAc-ZnO-NPs-150+ inoculated by *Rhizopus stolonifer* of tomato treatments, respectively. All management methods were affected by the storage period. pH declined compared to untreated fruits (control). Therefore, the change in pH might be due to the diversity in storage circumstances.

Table 4. Effect of different samples on pH of tomato fruits with *Rhizopus stolonifer* and under cold storage.

	pH (week)			
Sample	**1**	**2**	**3**	**4**
(Control)	3.5	2.6	1.8	1.4
Inoculated	2.5	1.8	1.1	1.1
CMC-g-PLAc-ZnO-NPs-150	3.4	2.4	1.6	1.3
CMC-g-PLAc-ZnO-NPs-150+ inoculated	2.8	1.9	1.4	1.2

Nanotechnology denotes a nanoscale technology which has a wide range of applications in a day to day life. Nanoscale science and nanotechnologies are intended to have the potential to develop agriculture and food project systems [58], and has given initiation to a new era of agro-nanotechnology. With the emergence and increase of microbial organisms resistant to many antibiotics and the continuing emphasis on healthcare costs, many scientists have examined a lot of experiments to improve new and effective antimicrobial reagents that do not excite resistance and are cost-effective solutions [59]. The cytotoxic mechanism of nanoparticles on microorganisms may result from the uptake of nanoparticles by cells since their particle sizes are smaller than the cell wall pores so they can penetrate their cell wall [60]. Another cytotoxicity may obtained from the ions released from the surface of the nanoparticles, as occurred in the case of CMC-g-PLAc-ZnO-NPs-150 [61], where the contact of bacterial cells to Zn ions induces changes in the cell membrane leading to the improvement of its permeability and consequent damage [62]. Nanoparticles may also create reactive oxygen species boosting membrane lipid peroxidation and consequent cell impairment. These mechanisms are also associated with the toxicity of the nanoparticles to biological systems, including eukaryotic cells [63]. The antimicrobial effect of zinc nanoparticles on fungi was accomplished due to generating reactive oxygen species NPs, causing deformed fungal hyphae with rapture and unusual bulges after zinc compounds treatment. Such morphological aberrations were associated with cell damage due to the excess production of reactive oxygen species, thus leading fungal cells to death [64]. Figure 12 (a-c) displays the SEM photomicrographs of CMC-g-PLAc-ZnO-NPs-150 that affected the mycelium growth, spore aggregation and shape malformation of *Rhizopus stolonifer*, demonstration photos of tomato fruit before treatment (control) and demonstration photo of tomato fruit after treatment by demonstration for 16 days, receptively. Through the results, it can be concluded that the existence of (*i.e.,* ZnO-NPs-150)

onto CMC-g-PLAc-ZnO-NPs-150 in the coated layer on the tomato fruits protects them for 16 days compared to the control one. Therefore, this CMC-g-PLAc-ZnO-NPs-150 nanocomposite films could be used to protect tomato fruits.

Figure 12. SEM photomicrographs of (a) CMC-g-PLAc-ZnO-NPs-150 affected the mycelium growth; (b) Spore development and shape malformation of *Rhizopus stolonifera*; (c) Photo of tomato before treatment (control); and (d) Photo of tomato after treatment by CMC-g-PLAc-ZnO-NPs-150 for 16 days. Radiation dose 10 kGy of radiation dose rate ~0.9 kGy/h.

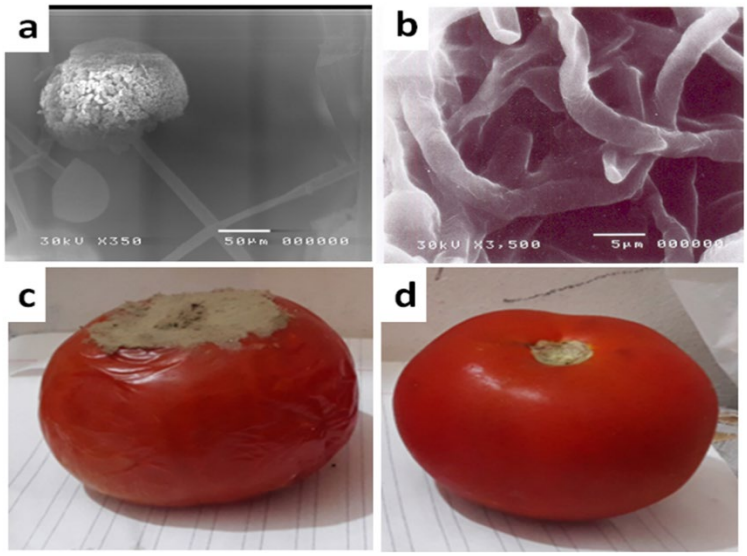

CONCLUSION

Various compositions of nanocomposites were prepared from (carboxymethylcellulose/polylactic acid) and Zinc Oxide Nanoparticles (ZnO-NPs) *via* gamma irradiation at radiation dose 10 kGy of radiation dose rate rate ~0.9 kGy/h. Nanoparticles of zinc oxide were synthesized. The nanocomposites of (carboxymethylcellulose/polylactic acid)/ZnO-NPs were characterized by FTIR, SEM, XRD, TEM, contact angle, Water Vapour Transmission Rate (WVRT) and mechanical properties. Advancement in nanotechnology has provided approaches to improve a reduction in crop spoilage and extend the shelf life of Tomato fruits and vegetables due to their antimicrobial activity. The present research's novelty is using CMC-g-PLAc-ZnO-NPs nanocompsoite films to reduce systematic resistance against tomato fruit rot caused by *Rhizopus stolonifer*. The obtained result showed that CMC-g-PLAc-ZnO-NPs-150 at 150 ppm in *in-vitro* prevented linear growth of *Rhizopus stolonifer*; also, in *in-vivo*, the same concentration prevented the severity of infection for three weeks below cold storage ambient temperature at 13°C and 90-95 relative humidity. The height firmness value of tomato fruits treated with CMC-g-PLAc-ZnO-NPs was followed by untreated samples (control). The lowest firmness values were those treated with CMC-g-PLAc-ZnO-NPs and inoculated, followed by inoculated samples with Rhizopus stolonifer after cold storage. Approximately the same result was obtained for (TSS) and pH. Scanning Electron Microscopy (SEM) approved the ultra-structure modification in *Rhizopus stolonifera* due to treatment by CMC-g-PLAc-ZnO-NPs impacted the mycelium growth and spore growth, and shape abnormality of *Rhizopus stolonifer* represents an aggregation of ZnO-NPs on mycelium, distortion and malformation.

ACKNOWLEDGEMENTS

We thank the National Center for Radiation Research and Technology (NCRRT) and Egyptian Atomic Energy Authority (EAEA) for the technical support.

DATA AVAILABILITY

Data generated or analysed during this study are provided in full within the published article.

COMPETING INTEREST

The authors declare no competing interest

RESEARCH FUNDING

None declared.

REFERENCES

1. FAO. Supporting sustainable fisheries and aquaculture. Food and Agriculture Organization. 2002.
2. Akogou FU, et al. Antimicrobial evaluation of red, phytoalexin rich sorghum food biocolorant. PLoS One. 2018;13:0194657.
3. Ameyapoh Y, et al. Hygienic quality of traditional processing and stability of tomato (*Lycopersicon esculentum*) puree in Togo. Bioresour Technol. 2008;9:5798-5803.
4. Liu Z, et al. Global cooling during the eocene-oligocene climate transition. Science. 2009;323:1187-1190.
5. Nunes MC, et al. Environmental conditions encountered during typical consumer retail display affect fruit and vegetable quality and waste. Postharvest Biol Tech. 2009;51:232-241.
6. Lee JY, et al. Extending shelf-life of minimally processed apples with edible coatings and antibrowning agents. Food Sci Technol. 2003;36:323-329.
7. Carrillo-Lopez A, et al. Ripening and quality changes in mango fruit as affected by coating with an edible film. J Food Qual. 2000;23:479-486.
8. Nimitkeatkai H, et al. Effect of edible coating on pineapple fruit quality during cold storage. Acta Hortic. 2006;712:643.
9. Kumbunleu J, et al. The study on chitosan coating on poly (lactic acid) film packaging to extend vegetable and fruit life. Conf Ser Mater Sci Eng. 2020;811:01202.
10. Homklin R, et al. Mechanical and thermal properties of PLA/PBS co-continuous blends adding nucleating agent. Energy Procedia. 2013;34:871.
11. Chen R, et al. Poly (lactic acid)/poly(butylene succinate)/calcium sulphate whiskers biodegradable blends prepared by vane extruder: Analysis of mechanical properties, morphology, and crystallization behaviour. J Qu Polym Test. 2014;34:1-9.
12. Zhang R, et al. Effect of PLA/PBAT antibacterial film on storage quality of passion fruit during the shelf-life. Molecules. 2019;24:3378.
13. Neugebauer D, et al. Synthesis of graft copolymers containing biodegradable poly (3-hydroxybutyrate) chains. Macromolecules. 2007;40:1767.
14. Fakhri LA, et al. Optimization of mechanical and colour properties of polystyrene/nanoclay/nano ZnO based nanocomposite packaging sheet using response surface methodology. Food Packing Shelf. 2018;17:11-24.
15. Jones N, et al. Antibacterial activity of ZnO nanoparticle suspensions on a broad spectrum of microorganisms. FEMS Microbiol Lett. 2007;279:71-76.

16. Jin T, et al. Antimicrobial efficacy of zinc oxide quantum dots against listeria monocytogenes, *Salmonella* enteritidis, and *Escherichia coli* 0157:H7. J Food Sci. 2009;74:46.
17. Abobatta WF, et al. Nanotechnology application in agriculture. Acta Sci Agric. 2018;26:99.
18. Park JH, et al. Antimicrobial spray nanocoating of supramolecular Fe(III)-tannic acid metal organic coordination complex: Applications to shoe insoles and fruits. Sci Rep. 2017;7:6980.
19. Thompson AK, et al. Postharvest technology of fruits and vegetables, harvesting, handling and storage. 2nd edition. Blackwell science publisher. New Jersey, United States. 2003;115-369.
20. Singh V, et al. Studies on Physico-chemical characteristics and processing quality of some tomato cultivars. Pharma Innova. 2021;10:2660.
21. Kumar VL, et al. The use of enzymes in food processing: A review. South Asian J Food Technol Environ. 2015;1:250.
22. Feliziani E, et al. Preharvest fungicide, potassium sorbate, or chitosan use on quality and storage decay of table grapes. Plant Dis. 2013;97:307-314.
23. Asmat-Campos D, et al. ZnO Nanoparticles obtained by green synthesis as an alternative to improve the germination characteristics of *L. esculentum*. Molecules. 2022;27:2343.
24. Mustapha S, et al. Comparative study of crystallite size using Williamson-Hall and Debye-Scherrer plots for ZnO nanoparticles. Nanosci Nanotechnol Lett. 2019;10:045013.
25. Gunathilake SU, et al. pH responsive poly(lactic acid)/sodium carboxymethyl cellulose film for enhanced delivery of curcumin *in vitro*. J Drug Deliv Sci Technol. 2020;58:10178.
26. Fekete T, et al. Synthesis of carboxymethylcellulose/starch superabsorbent hydrogels by gamma-irradiation. Chem Cent J. 2017;11:46.
27. Coudane J, et al. Poly (lactic acid) based graft copolymers: Syntheses strategies and improvement of properties for biomedical and environmentally friendly applications: A review. Molecules. 2022;27:4135.
28. Coudane J, et al. Poly (lactic acid)-based graft copolymers: syntheses strategies and improvement of properties for biomedical and environmentally friendly applications: A review. Molecules. 2022;27:4135.
29. Demeter M, et al. State of the art of hydrogel wound dressings developed by ionizing radiation. Gels. 2023;9:55.
30. Gams W, et al. CBS course of mycology. 4th edition. Centraalbureau Voor Schimmelcultures Publisher. Baarn, Netherlands. 1998.
31. Chastanger GA, et al. A fungicide wax treatment to suppress botrytis cinerea and protect fresh market tomatoes. Phytopathol. 1979;69:59.
32. AOAC. Official methods of analysis of the association of official analytical chemists. 14th edition. Washington, D.C. USA. 1995;125.
33. Harley MM, et al. The role of SEM in pollen morphology and plant systematic. Clarendon press. oxford, USA. 1991:41-45.
34. Singh P, et al. Assessment of *Pelargonium graveolens* oil as plant based antimicrobial and aflatoxin suppressor in food preservation. J Sci Food Agric. 2008;88:2421-2425.
35. Ahmed W, et al. Effect of Ni doping on structural, optical and magnetic characteristics of ZrO_2 nanoparticles with efficient visible light driven photocatalytic activity. Ceram Int. 2012;47:24895.
36. Reddy AJ, et al. Structural, optical and EPR studies on ZnO:Cu nanopowders prepared via low temperature solution combustion synthesis. J Alloys Comp. 2011;509:5349.
37. Arshad M, et al. Effect of Co substitution on the structural and optical properties of ZnO nanoparticles synthesized by sol–gel route. J Alloys Comp. 2011;509:8378.
38. Zak AK, et al. Synthesis and characterization of a narrow size distribution of zinc oxide nanoparticles. Int J Nanomedicine.

2011;6:1399.

39. Brunner E, et al. Chitin based scaffolds are an integral part of the skeleton of the marine demosponge *Ianthella basta*. J Struct Biol. 2009;168:539.
40. Focher B, et al. Structural differences between chitin polymorphs and their precipitates from solutions evidence from CP-MAS ^{13}C-NMR, FT-IR and FT-Raman spectroscopy. Carbohydr Polym. 1992;17:97.
41. Au HT, et al. Fabrication of an antibacterial non-woven mat of a poly(lactic acid)/chitosan blend by electro spinning. Macromol Res. 2012;20:51.
42. Xu J, et al. Preparation of chitosan/PLA blends micro/nanofibers by electrospinning. J Mater Lett. 2009;63:658.
43. Zhao J, et al. Size controlled synthesis of ZnO nanoparticles and their photoluminescence properties. J Lumin. 2007;122:195.
44. Khoshhesab ZM, et al. Preparation of ZnO nanostructures by chemical precipitation method. Nano-Met Chem. 2011;41:814.
45. JCPDS. Powder diffraction file, alphabetical index, inorganic compounds. International Centre for Diffraction Data. Newtown Square, USA. 1977.
46. Cullity BD, et al. Elements of X-Ray diffraction. 3rd edition. Addison-Wesley publisher. Newyork, USA. 1967.
47. Dwivedi J, et al. Electrospun nanofibrous scaffold as a potential carrier of antimicrobial therapeutics for diabetic wound healing and tissue regeneration. Elsevier. Newyork, USA. 2017;147-164.
48. Jeong S, et al. *In situ* real time monitoring technologies for fouling detection in membrane processes. Biotechnol Bioeng. 2023:43-64.
49. Kim I, et al. Poly (lactic acid)/ZnO bionanocomposite films with positively charged ZnO as potential antimicrobial food packaging materials. J Polymers. 2019;11:1427.
50. Ni S, et al. ZnO nanoparticles enhanced hydrophobicity for starch film and paper. Mater Lett. 2018;230:207-210.
51. Bhatti MA, et al. Efficient photo catalysts based on silver doped ZnO nanorods for the photo degradation of methyl orange. Ceram Int. 2019;45:23289–23297.
52. Channa IA, et al. UV blocking and oxygen barrier coatings based on polyvinyl alcohol and zinc oxide nanoparticles for packaging applications. Coatings. 2022;12:897.
53. Lee SW, et al. The effects of zinc oxide nanoparticles on the physical, mechanical and antimicrobial properties of chicken skin gelatin/tapioca starch composite films in food packaging. J Food Sci Technol. 2020; 58:4294-4302.
54. Marvizadeh MM, et al. Preparation and characterization of bionanocomposite film based on tapioca starch/bovine gelatin/nanorod zinc oxide. Int J Biol Macromol. 2017;99:1–7.
55. Rhim JW, et al. Effect of clay contents on mechanical and water vapour barrier properties of agar based nanocomposite films. Carbohydr Polym. 2011;86:691–699.
56. Kumar P, et al. Preparation and characterization of bio-nanocomposite films based on soy protein isolate and montmorillonite using melt extrusion. J Food Eng. 2010;100:480–489.
57. Sahraee S, et al. Physicochemical and antifungal properties of bio-nanocomposite film based on gelatin-chitin nanoparticles. Int J Biol Macromol. 2017;97:373–381.
58. Seil JT, et al. Antimicrobial applications of nanotechnology: Methods and literature. Int J Nanomedicine. 2012;7:2767.
59. Dunne WM, et al. Next generation and whole genome sequencing in the diagnostic clinical microbiology laboratory. Eur J Clin Microbiol Infect Dis. 2012;31:1719.
60. Moritz M, et al. The newest achievements in synthesis, immobilization and practical applications of antibacterial nanoparticles. Chem Eng J. 2013;228:596.

61. Rai M, et al. Silver nanoparticles as a new generation of antimicrobials. Biotech Adv. 2009;27:76.
62. Barani H, et al. *In situ* synthesis of nano silver/lecithin on wool: Enhancing nanoparticles diffusion. Biointerfaces. 2012;92:9.
63. Bondarenko O, et al. Toxicity of Ag, CuO and ZnO nanoparticles to selected environmentally relevant test organisms and mammalian cells *in vitro*: A critical review. Arch Toxicol. 2013;87:1181.
64. Savi GD, et al. Antifungal properties of Zinc compounds against toxigenic fungi and mycotoxin. Int J Food Sci. 2013;48:1834.